Journal of the Physical Society of Japan
Vol. 76, No. 3, March, 2007, 034711

Massless Fermions in Organic Conductor

Akito KOBAYASHI[1,2], Shinya KATAYAMA[2],
Yoshikazu SUZUMURA[2], and Hidetoshi FUKUYAMA[3]

[1]*Institute for Advanced Research, Nagoya University, Furo-cho, Chikusa-ku, Nagoya 464-8602*
[2]*Department of Physics, Nagoya University, Furo-cho, Chikusa-ku, Nagoya 464-8602*
[3]*Department of Applied Physics, Tokyo University of Science, 1-3 Kagurazaka, Shinjuku-ku, Tokyo 162-8601*

(Received December 16, 2006; accepted January 10, 2007; published March 12, 2007)

The electronic states in two-dimensional organic conductor α-(BEDT-TTF)$_2$I$_3$ have been investigated to show the noticeable property of the massless fermions, i.e., the linear dispersion which exists on the contact point between the conduction band and the valence band. These fermions are well known in bismuth and graphite, where the former are described by the Dirac equation and the latter obeys the Weyl equation corresponding to the massless fermion. In the present study, we show that the effective Hamiltonian describing the massless fermions in α-(BEDT-TTF)$_2$I$_3$ contains intrinsically new terms of Pauli matrices σ_z and σ_0 in addition to the Weyl equation which consists of σ_x and σ_y. The new massless fermions are robust against the charge disproportionation, and induce the anomalous momentum-dependence in the charge density.

KEYWORDS: massless fermion, Dirac equation, Weyl equation, α-(BEDT-TTF)$_2$I$_3$, charge disproportionation
DOI: 10.1143/JPSJ.76.034711

1. Introduction

The massless fermions in condensed matter physics, which display the linear dispersion of the energy band in the vicinity of the contact point between the conduction band and the valence band,[1)] have been studied in bismuth[2–4)] and graphite[5–10)] showing anomalous properties, e.g. the anomalous diamagnetism, the absence of the backward scattering and the universal conductivity. The fermions in bismuth are described by the Dirac equation with the Hamiltonian which consists of 4×4 components.[2)] The fermions in graphite obey the Weyl equation for neutrino,[5,6)] which is derived from the Dirac equation without rest mass, and consists of σ_x term and σ_y term.

In two-dimensional organic conductor α-(BEDT-TTF)$_2$I$_3$, the zero-gap state (ZGS) with the massless fermions was found theoretically,[11,12)] by using the transfer integrals[13)] calculated from the experimental data under uniaxial strain. The characteristic of the ZGS is the existence of the contact point on the Fermi surface, which is located between the conduction band and the valence band. The ZGS was verified by the first principle calculation.[14,15)] The puzzled phenomena of the weak temperature dependence of resistivity and the strong T^2 dependence of carrier density, which were discussed as the narrow gap semiconductor,[16,17)] have been explained by applying the self-consistent Born approximation to the ZGS.[18)] In addition to ZGS, there are several interesting phenomena in α-(BEDT-TTF)$_2$I$_3$. The stripe charge ordering, which occurs at low pressures,[19)] has been explained by the mean-field theories.[20–22)] For the superconductivity, which is found in the presence of the stripe charge ordering under uniaxial pressure,[23)] has been investigated by using the extended Hubbard model.[24)] The paring mechanism which is mediated by the spin fluctuation has been maintained and interpreted in terms of the self-doped pseduo-one-dimenstional Heisenberg chain. Recently, the charge disproportionation has been observed at temperature higher than the transition temperature of the stripe charge ordering.[25)] We examine the effect of charge disproportionation on electronic state of the massless fermion by calculating the momentum dependence of charge density of the respective site.

In the present study, the electronic states of the massless fermions in α-(BEDT-TTF)$_2$I$_3$ are investigated. The extended Hubbard model describing α-(BEDT-TTF)$_2$I$_3$ is given and is treated by the mean-field theory in §2. In §3, we show that the Hamiltonian describing the massless fermions has intrinsically new terms of σ_z and the identity matrix σ_0 in addition to the Weyl equation which consists of σ_x and σ_y. In §4, we show the robust stability of the massless fermion against the charge disproportionation, which originates from the variety of transfer integrals. In §5, we calculate the anomalous momentum-dependence of the charge density, which is related to both the massless fermion and the charge disproportionation. In §6, the anomaly on the contact point is discussed in terms of the wave function of the massless fermions and summary is given.

2. Hamiltonian and Mean-Field Theory

The model describing the two-dimensional electronic system in the α-(BEDT-TTF)$_2$I$_3$ is shown in Fig. 1.[26)] The unit cell consists of four BEDT-TTF molecules with sites 1, 2, 3, and 4, which correspond to sites A, A′, B and C in the conventional notation.[19)] There are six electrons in the four molecules, i.e., the 3/4-filled band. The extended Hubbard model with the on-site repulsive interaction U and the anisotropic nearest-neighbor repulsive interaction $V_{\alpha\beta}$ is given by[11)]

$$\begin{aligned} H = & \sum_{(i\alpha;j\beta),\sigma} (t_{i\alpha;j\beta} a^\dagger_{i\alpha\sigma} a_{j\beta\sigma} + \text{h.c.}) \\ & + \sum_{i\alpha} U a^\dagger_{i\alpha\uparrow} a^\dagger_{i\alpha\downarrow} a_{i\alpha\downarrow} a_{i\alpha\uparrow} \\ & + \sum_{(i\alpha;j\beta),\sigma,\sigma'} V_{\alpha\beta} a^\dagger_{i\alpha\sigma} a^\dagger_{j\beta\sigma'} a_{j\beta\sigma'} a_{i\alpha\sigma}, \end{aligned} \tag{1}$$

where i, j denote site indices of the unit cell, and α, β $(= 1, 2, 3, 4)$ are indices of BEDT-TTF sites in the unit cell. Hereafter, we take eV as the unit of the energy. In the first

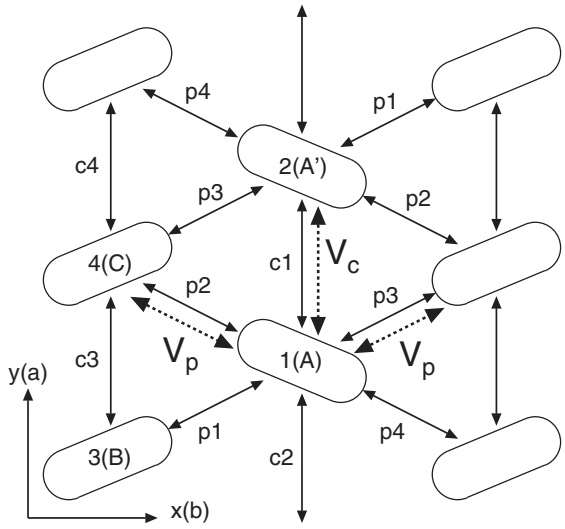

Fig. 1. The model describing the electronic system of α-(BEDT-TTF)$_2$I$_3$. The unit cell consists of four BEDT-TTF molecules 1, 2, 3, and 4 with seven transfer integrals t_A. The the nearest neighbor repulsive interactions are given by V_c and V_p. The a- and b-axes in the conventional notation correspond to the y- and x-axes in the present paper.

term, $a^\dagger_{i\alpha\sigma}$ denotes a creation operator with spin σ ($=\uparrow,\downarrow$) and $t_{i\alpha;j\beta}$ is the transfer energy between the (i,α) site and the (j,β) site. The transfer integrals under the uniaxial pressure (P_a) along the a-axis is obtained by the extrapolation formula

$$t_A(P_a) = t_A(0)(1 + K_A P_a). \tag{2}$$

The transfer energies t_A with $A = c1, c2, \ldots, p4$ and the coefficients K_A are given by the data at $P_a = 0$ kbar[27] and at $P_a = 2$ kbar,[13] where $t_{p1}(0) = 0.140$, $t_{p2}(0) = 0.123$, $t_{p3}(0) = -0.025$, $t_{p4}(0) = -0.062$, $t_{c1}(0) = 0.048$, $t_{c2}(0) = -0.020$, $t_{c3}(0) = -0.028$, $t_{c4}(0) = -0.028$, and $K_{p1} = 0.011$, $K_{p2} = 0$, $K_{p3} = 0$, $K_{p4} = 0.032$, $K_{c1} = 0.167$, $K_{c2} = -0.025$, $K_{c3} = 0.089$.

The charge ordering is estimated within the mean field theory[11,20,21] given by

$$H_{MF} = \sum_{\mathbf{k}\alpha\beta\sigma} \tilde{\epsilon}_{\alpha\beta\sigma}(\mathbf{k}) a^\dagger_{\mathbf{k}\alpha\sigma} a_{\mathbf{k}\beta\sigma} - \sum_\alpha U_\alpha \langle n_{\alpha\uparrow}\rangle \langle n_{\alpha\downarrow}\rangle - \sum_{\langle\alpha,\beta\rangle\sigma,\sigma'} V_{\alpha\beta} \langle n_{\alpha\sigma}\rangle \langle n_{\beta\sigma'}\rangle, \tag{3}$$

$$\tilde{\epsilon}_{\alpha\beta\sigma}(\mathbf{k}) = \delta_{\alpha\beta}[U_\alpha \langle n_{\alpha\bar{\sigma}}\rangle + \sum_{\beta'\sigma'} V_{\alpha\beta'} \langle n_{\beta'\sigma'}\rangle] + \epsilon_{\alpha\beta}(\mathbf{k}), \tag{4}$$

$$\epsilon_{\alpha\beta}(\mathbf{k}) = \sum_\delta t_{\alpha\beta} e^{i\mathbf{k}\cdot\delta}, \tag{5}$$

where $n_{\alpha\sigma} = a^\dagger_{i\alpha\sigma} a_{i\alpha\sigma}$ (i.e., independent of the site i), $\bar{\sigma} = -\sigma$, and δ denotes the vector representing the nearest neighbor of the unit cell. The Hamiltonian (3) is diagonalized by

$$\sum_{\beta=1}^{4} \tilde{\epsilon}_{\alpha\beta\sigma}(\mathbf{k}) d_{\beta r\sigma}(\mathbf{k}) = \xi_{r\sigma}(\mathbf{k}) d_{\alpha r\sigma}(\mathbf{k}), \tag{6}$$

where $\xi_{r\sigma}$ are the eigenvalue with a descending order, $\xi_{1\sigma}(\mathbf{k}) > \xi_{2\sigma}(\mathbf{k}) > \xi_{3\sigma}(\mathbf{k}) > \xi_{4\sigma}(\mathbf{k})$, and $d_{\alpha r\sigma}(\mathbf{k})$ ($r = 1,2,3,4$) are the corresponding eigenvectors. In terms of eq. (6), the number of electrons on α-site with spin σ, $\langle n_{\alpha\sigma}\rangle$, is expressed as

$$\langle n_{\alpha\sigma}\rangle = \sum_{r=1}^{4} d^*_{\alpha r\sigma}(\mathbf{k}) d_{\alpha r\sigma}(\mathbf{k}) \frac{1}{\exp[(\xi_{r\sigma}(\mathbf{k}) - \mu)/T] + 1}, \tag{7}$$

where T is the temperature ($k_B = 1$). Equation (7) is the self-consistency equation for $\langle n_{\alpha\sigma}\rangle$. The quantity μ is the chemical potential determined from a condition

$$\frac{3}{2} = \frac{1}{4} \sum_{\alpha\sigma} \langle n_{\alpha\sigma}\rangle. \tag{8}$$

which gives the electron with 3/4 filling per each molecule.

The mean-field solutions are as follows.[24] The zero-gap state (ZGS) accompanied by the charge disproportionation exists in the region of high pressure ($P_a > 4.3$ kbar). There are insulator phase ($0 \le P_a < 3.3$ kbar) and the metallic phase ($3.3 \le P_a < 4.3$ kbar) accompanied by the stripe charge ordering in the region of lower pressure. The superconductivity in the presence of the stripe charge ordering, which is mediated by the spin fluctuation, occurs in the metallic phase. The parameters $U = 0.4$, $V_c = 0.17$, and $V_p = 0.05$ are chosen so that the stripe pattern is consistent with that of the experiment.[19] The electronic states which vary with increasing P_a reproduce well those of the experiment.[23]

3. Massless Fermions

Figure 2 shows the energy bands with the linear dispersion in the vicinity of the contact point $\mathbf{k}_0$ at which the conduction band (the electron band) and the valence band (the hole band) degenerate,[12] i.e., so-called the massless fermions. The Fermi energy coincides with the energy of the contact point. This state has been called as the ZGS.

In the present study, we investigate the electronic states in the vicinity of the contact point. By making use of the expansion with respect to $\tilde{\mathbf{k}}$ ($= \mathbf{k} - \mathbf{k}_0$), the Hamiltonian around the contact point $\mathbf{k}_0$ is given as

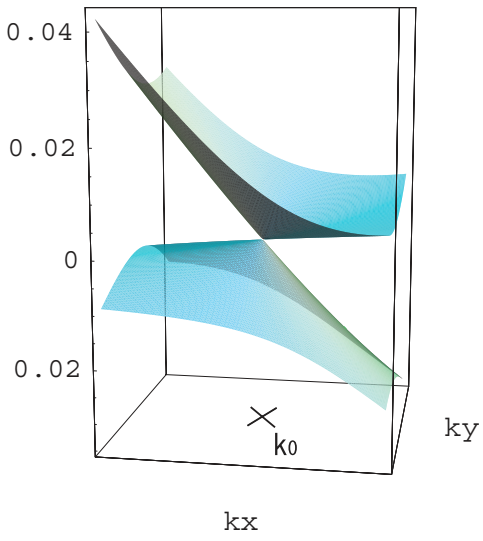

Fig. 2. The massless fermions in α-(BEDT-TTF)$_2$I$_3$. The vertical axis represents the band energy (eV), on the k_x–k_y plane ($k^0_x - 0.1\pi \le k_x \le k^0_x + 0.1\pi$ and $k^0_y - 0.1\pi \le k_y \le k^0_y + 0.1\pi$), where the contact point is given by $\mathbf{k}_0 = (0.740\pi, -0.346\pi)$ at $P_a = 4.5$ kbar, $U = 0.4$, $V_c = 0.17$, and $V_p = 0.05$. The upper (lower) cone corresponds to the conduction ξ_1 (valence ξ_2) band. The Fermi energy coincides with the contact point in the ZGS. Another contact point with $\mathbf{k} = -\mathbf{k}_0$ also has the massless fermions.

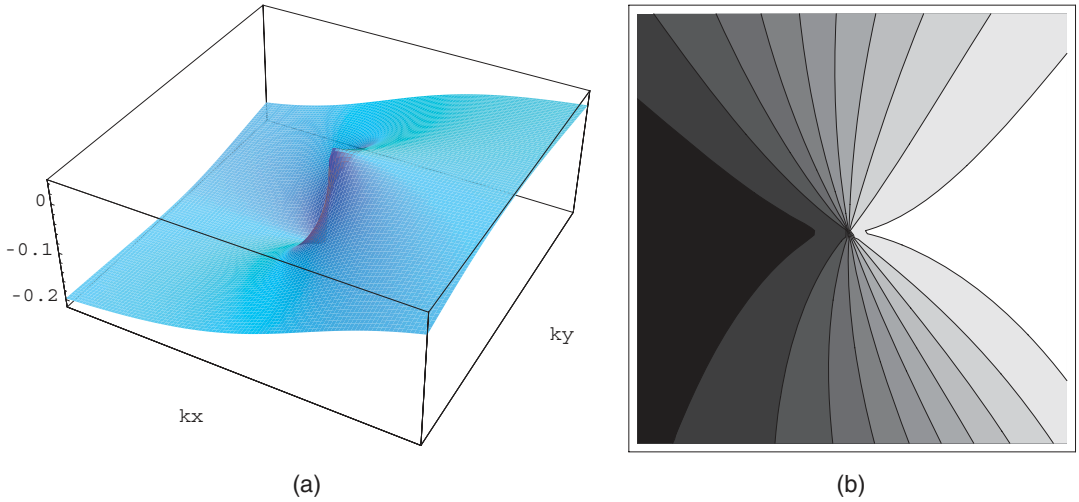

Fig. 3. The momentum dependence of $u^x_{11}(\mathbf{k})$ (a) and the contour plot (b) in the region ($k^0_x - 0.1\pi \le k_x \le k^0_x + 0.1\pi$ and $k^0_y - 0.1\pi \le k_y \le k^0_y + 0.1\pi$) at $P_a = 4.5$ kbar. There is anti-symmetric component around $\mathbf{k}_0$ with a discontinuous jump at $\mathbf{k}_0$.

$$H(\mathbf{k}) = H(\mathbf{k}_0) + H'(\tilde{\mathbf{k}}), \tag{9}$$

$$H'(\tilde{\mathbf{k}}) = \tilde{\mathbf{k}} \cdot \nabla H(\mathbf{k}_0) \tag{10}$$

For H', we take the effective Hamiltonian represented in terms of 2×2 components for the conduction band ($\gamma = 1$) and the valence band ($\gamma = 2$), because the linear components are dominant at $\mathbf{k}_0$ and the components related to the other bands ($\gamma = 3$ or 4) are negligible. By using the velocity matrix $\mathbf{u}_{\gamma\gamma'}(\mathbf{k})$ given as

$$u^\tau_{\gamma\gamma'}(\mathbf{k}) = \sum_{\alpha\beta} d^*_{\alpha\gamma}(\mathbf{k}) d_{\beta\gamma'}(\mathbf{k}) \frac{\partial \tilde{\epsilon}_{\alpha\beta}(\mathbf{k})}{\partial k_\tau}, \tag{11}$$

where $\tau = x, y$ and $\gamma, \gamma' = 1, 2$, the velocities $\mathbf{v}_\rho(\mathbf{k})$ are defined as

$$\mathbf{v}_x(\mathbf{k}) = \mathrm{Re}\, \mathbf{u}_{12}(\mathbf{k}), \tag{12}$$

$$\mathbf{v}_y(\mathbf{k}) = -\mathrm{Im}\, \mathbf{u}_{12}(\mathbf{k}), \tag{13}$$

$$\mathbf{v}_z(\mathbf{k}) = \frac{1}{2}(\mathbf{u}_{11}(\mathbf{k}) - \mathbf{u}_{22}(\mathbf{k})), \tag{14}$$

$$\mathbf{v}_0(\mathbf{k}) = \frac{1}{2}(\mathbf{u}_{11}(\mathbf{k}) + \mathbf{u}_{22}(\mathbf{k})), \tag{15}$$

respectively. All the components of $\mathbf{v}_\rho(\mathbf{k})$ ($\rho = x, y, z, 0$) are of the same order. The effective Hamiltonian H_{eff} can be expressed as[28]

$$H_{\mathrm{eff}}(\tilde{\mathbf{k}}) = \sum_{\rho=x,y,z,0} \tilde{\mathbf{k}} \cdot \mathbf{v}_\rho(\mathbf{k}'_0)\sigma_\rho, \tag{16}$$

where $\sigma_{x,y,z}$ are the Pauli matrices and σ_0 is the identity matrix. Since $\mathbf{u}_{\gamma\gamma'}(\mathbf{k})$ are singular at $\mathbf{k}_0$ [see Fig. 3(a)], we introduce a momentum $\mathbf{k}'_0$ which is infinitesimally different from the contact point $\mathbf{k}_0$. The direction of $\mathbf{k}'_0 - \mathbf{k}_0$ is arbitrary. The linear dispersion $\xi_{\mathrm{eff}}(\tilde{\mathbf{k}})$ with a cone is obtained by diagonalization of H_{eff}.

$$\xi_{\mathrm{eff}}(\tilde{\mathbf{k}}) = \tilde{\mathbf{k}} \cdot \mathbf{v}_0(\mathbf{k}'_0) \pm \sqrt{\sum_\nu (\tilde{\mathbf{k}} \cdot \mathbf{v}_\nu(\mathbf{k}'_0))^2} \tag{17}$$

$$= \sum_\tau \tilde{k}_\tau v^\tau_0(\mathbf{k}'_0) \pm \sqrt{\sum_{\tau\tau'} \tilde{k}_\tau \tilde{k}_{\tau'} Q^{\tau\tau'}(\mathbf{k}'_0)}, \tag{18}$$

where $Q^{\tau\tau'} = 4\sum_\nu v^\tau_\nu v^{\tau'}_\nu$ and $\nu = x, y, z$. Although eq. (16) depends on the direction of $\mathbf{k}'_0 - \mathbf{k}_0$, the eigenvalues $\xi_{\mathrm{eff}}(\tilde{\mathbf{k}})$ are independent of the choice of $\mathbf{k}'_0$. Here we note that the

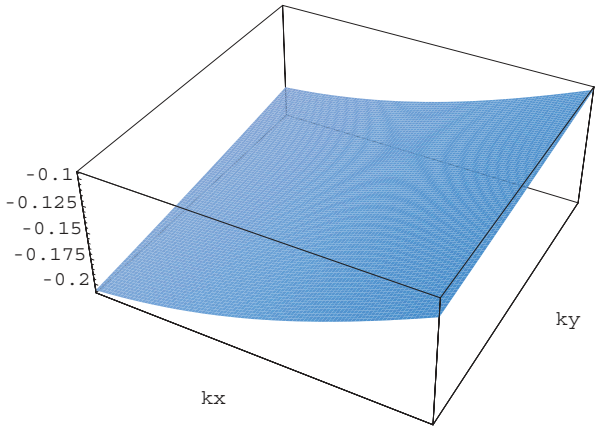

Fig. 4. The momentum dependence of $u^x_{11}(\mathbf{k}) + u^y_{22}(\mathbf{k})$ in the region of $k^0_x - 0.1\pi \le k_x \le k^0_x + 0.1\pi$ and $k^0_y - 0.1\pi \le k_y \le k^0_y + 0.1\pi$. The strong momentum dependences of $u^x_{11}(\mathbf{k})$ and $u^y_{22}(\mathbf{k})$ cancel each other completely.

Hamiltonian describing the massless fermions in graphite consists of σ_x and σ_y terms with $\mathbf{v}_x = (v, 0)$ and $\mathbf{v}_y = (0, v)$ and then obeys the Weyl equation for the neutrino. The Weyl equation is obtained by vanishing rest mass term of the relativistic Dirac equation which consists of 4×4 components.[4,7] In eq. (16), new terms of σ_z and σ_0 are added to the Weyl equation. The term of σ_0 leads to the anisotropic velocity. Thus H_{eff} in eq. (16) gives new massless fermions which have the anisotropy of the velocity and the inclination of the cone. In addition, the corresponding quantity on another contact point at $-\mathbf{k}_0$ shows a fact that $\mathbf{v}_\rho(-\mathbf{k}_0 + \delta\mathbf{k}) = -\mathbf{v}_\rho(\mathbf{k}_0 - \delta\mathbf{k})$ due to the crystal symmetry.

The velocity matrix $\mathbf{u}_{\gamma\gamma'}(\mathbf{k})$ has anomalous momentum dependence around $\mathbf{k}_0$. Figures 3(a) and 3(b) show the momentum dependence of $u^x_{11}(\mathbf{k})$ in the vicinity of $\mathbf{k}_0$ ($k^0_x - 0.1\pi \le k_x \le k^0_x + 0.1\pi$ and $k^0_y - 0.1\pi \le k_y \le k^0_y + 0.1\pi$). There are anti-symmetric component around $\mathbf{k}_0$ with a discontinuous jump at $\mathbf{k}_0$. The anomaly comes from the property of the wave function of the massless fermion (discussed in §6). The anomaly in the momentum dependence of $\mathbf{u}_{\gamma\gamma'}(\mathbf{k})$ cancels completely for $\mathbf{v}_0(\mathbf{k})$ as shown in

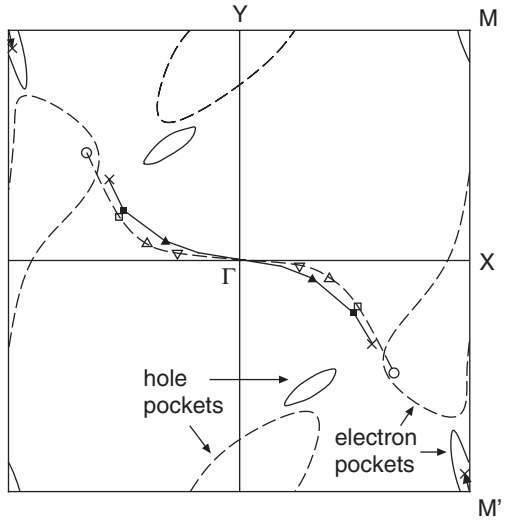

Fig. 5. The solid curves show trajectories of a pair of the contact points $\pm\mathbf{k}_0$ which move to the Γ-point each other with increasing P_a, where $U = 0.4$, $V_c = 0.17$, and $V_p = 0.05$. The small ellipse of solid line represents the electron and hole pockets for the metallic state at $P_a = 4$ kbar. The dashed curves are obtained for the non-interacting case. The contact points also move form open-circle points ($P_a = 0$ kbar) to the Γ-point. The dashed curves around the X- and Y-points represent the electron and hole pockets at $P_a = 0$. The square, triangle and inverted triangle points correspond to $P_a = 10$, 20, and 30 kbar, respectively.

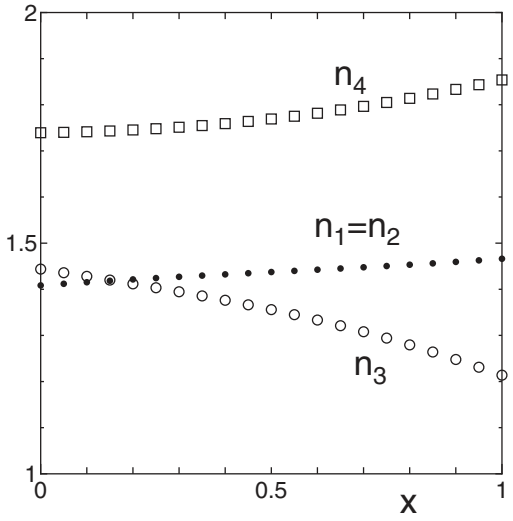

Fig. 6. The x-dependences of n_α ($= \sum_\sigma n_{\alpha\sigma}$), where $U = 0.4x$, $V_c = 0.17x$, and $V_p = 0.05x$, at $P_a = 4.5$ kbar.

Fig. 4 in the vicinity of $\mathbf{k}_0$ ($k_x^0 - 0.1\pi \le k_x \le k_x^0 + 0.1\pi$ and $k_y^0 - 0.1\pi \le k_y \le k_y^0 + 0.1\pi$), where $u_{11}^x(\mathbf{k}) + u_{22}^x(\mathbf{k}) = 2v_0^x(\mathbf{k})$. For example, we obtain fixed values $\mathbf{v}_0(\mathbf{k}_0) = (-8.21 \times 10^{-2}, -1.29 \times 10^{-2})$ (eV with the lattice constant $a = b = 1$) at $P_a = 4.5$ kbar.

The anomaly of $\mathbf{v}_\nu(\mathbf{k})$ ($\nu = x, y, z$) is understood from the property of the rotation of these vectors. When $\mathbf{k}$ goes counterclockwise around $\mathbf{k}_0$, these vectors also rotate counterclockwise, with the variation of the magnitude of these vectors. The anomaly in $\mathbf{v}_\nu(\mathbf{k})$ vanish in $Q^{\tau\tau'}(\mathbf{k})$ completely. Then we obtain fixed values $Q^{xx}(\mathbf{k}_0) = 4.40 \times 10^{-2}$, $Q^{xy}(\mathbf{k}_0) = Q^{yx}(\mathbf{k}_0) = 1.15 \times 10^{-2}$ and $Q^{yy}(\mathbf{k}_0) = 3.34 \times 10^{-2}$ at $P_a = 4.5$ kbar.

In order to see the degree of anisotropy, we rotate $\tilde{k}_x$- and $\tilde{k}_y$-axis to $\tilde{K}_x$ and $\tilde{K}_y$-axis to take the principal axis of the ellipse. Thus we obtain

$$\sum_{\tau\tau'} \tilde{k}_\tau \tilde{k}_{\tau'} Q^{\tau\tau'}(\mathbf{k}_0) = A_x^2 \tilde{K}_x^2 + A_y^2 \tilde{K}_y^2, \tag{19}$$

where $A_x = 0.227$, $A_y = 0.161$, and the rotational angle of the axis is given by $\theta = -0.568$ rad.

Figure 5 shows the trajectories of the contact points with varying P_a, which are calculated by the extrapolation in the tight-binding model [eq. (2)] with increasing P_a. The contact point emerges at M'-point which corresponds to the metallic phase accompanied by the stripe charge ordering. The point moves from M'-point ($P_a = 3.3$ kbar) to the cross (×)-point ($P_a = 4.3$ kbar), where the Fermi energy does not coincide with the contact point. The contact point in the ZGS jumps into another cross (×)-points ($P_a = 4.3$ kbar) and moves toward the Γ-point. The dashed curves are obtained for the non-interacting case, where the contact point also moves form open-circle point ($P_a = 0$ kbar) toward the Γ-point. A pair of the contact points at $\pm\mathbf{k}_0$ approaching the Γ-point each other vanish due to collision at $P_a \cong 40$ kbar. The electronic system becomes the band insulator at pressures higher than $P_a \cong 40$ kbar. For pressures just before the collision, the anisotropy of the velocity and the inclination of the cone are strongly enhanced, and two Van Hove singularities approach the Fermi energy each other.

4. Charge Disproportionation vs Massless Fermion

We investigate the origin of the charge disproportionation observed in α-(BEDT-TTF)$_2$I$_3$.[25] Figure 6 shows the charge disproportionation as the function of the magnitude of the interactions U, V_p, and V_c, which are chosen as $U = 0.4x$, $V_c = 0.17x$, and $V_p = 0.05x$ (eV). The case of $x = 1$ corresponds to the ZGS which describes the real material at $P_a = 4.5$ kbar, while the case of $x = 0$, on the other hand, corresponds to that of the tight-binding model. It is found that the charge disproportionation does exist even at $x = 0$. Thus, the charge disproportionation originates from the transfer integrals. The disproportionation is enhanced as x decreases.

The presence of the interactions ($x = 1$) gives spatial variation observed by the NMR experiment,[25] that the site 3 is hole-rich and the site 4 is electron-rich among four sites. The stability of the massless fermions against the charge disproportionation is evidenced by the fact that the ZGS is found in whole range ($0 \le x \le 1$) of the solutions.

Figure 7 shows the temperature-dependences of n_α ($\alpha = 1, 2, 3, 4$) for $x = 1$ at $P_a = 0$. The insulating state accompanied by the stripe charge ordering is obtained in the region of low temperature $T < T_{CO} = 0.016$. There are large staggered magnetic moments m_1 (> 0) and m_3 (< 0) on the hole-rich sites for $T < T_{CO}$, where $m_\alpha = \sum_\sigma \mathrm{sgn}(\sigma) n_{\alpha\sigma}$. At high temperature regions ($T > T_{CO}$), on the other hand, there is the metallic state accompanied by the charge disproportionation, where the magnetic moments m_α vanish. In the metallic state, the contact point leaves the Fermi energy because of the appearance of the hole pocket at Y-point. It is found that there is no critical temperature for the vanishing of the charge disproportionation even in the case of $x = 1$. The stability of the massless fermions against

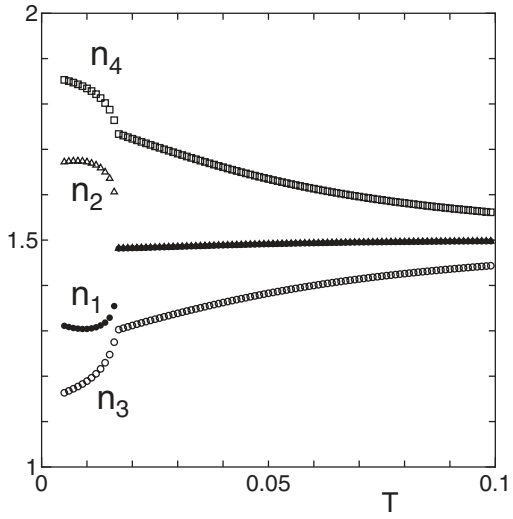

Fig. 7. The temperature-dependences of n_1, n_2, n_3, and n_4 at $P_a = 0$ kbar for $x = 1$.

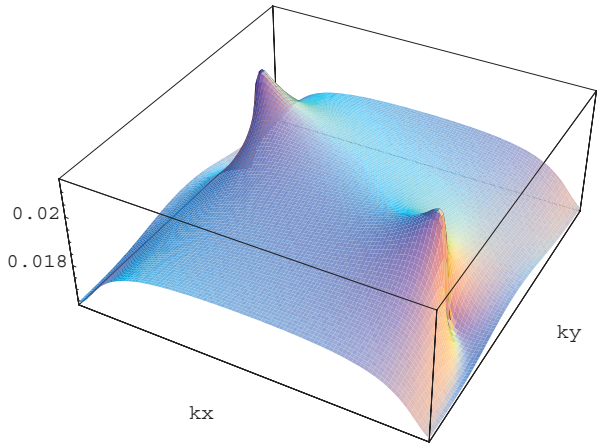

Fig. 8. The momentum-dependence of $n_1(\mathbf{k})$ [$= n_2(\mathbf{k})$] in the 1st Brillouin zone.

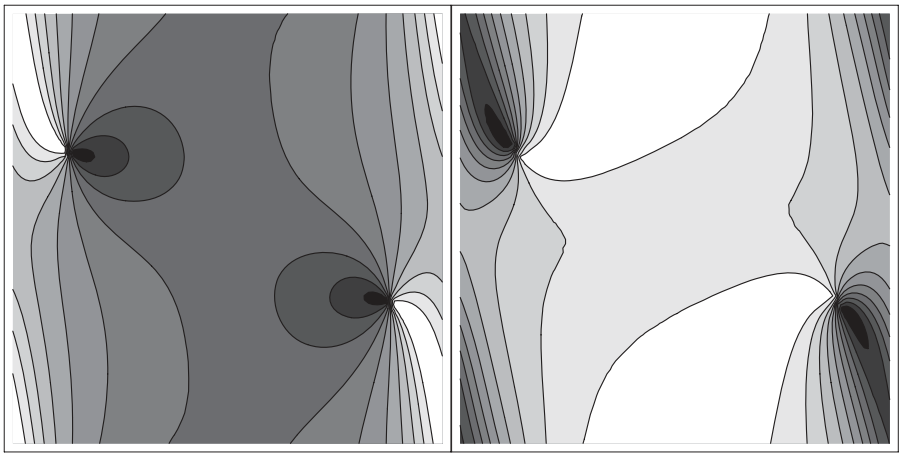

Fig. 9. The contour plots of the momentum-dependence of $n_3(\mathbf{k})$ (left) and $n_4(\mathbf{k})$ (right) in the 1st Brillouin zone, where $n_\alpha(\mathbf{k})$ is large (small) in the light (dark) region.

the charge disproportionation is also verified since the massless fermions are obtained in this metallic state ($T > T_{\rm CO}$).

5. Anomalous Momentum-Dependence of Charge Density

We examine the anomaly in the momentum-dependence of the charge density $n_\alpha(\mathbf{k})$ for each BEDT-TTF site (per spin) which is given by ($k_{\rm B} = 1$)

$$n_\alpha(\mathbf{k}) = \sum_\gamma d^*_{\alpha\gamma}(\mathbf{k}) d_{\alpha\gamma}(\mathbf{k}) \frac{1}{\exp(\xi_\gamma(\mathbf{k})/T) + 1}. \quad (20)$$

Figure 8 shows the momentum-dependence of $n_1(\mathbf{k})$ [$= n_2(\mathbf{k})$]. It is found that the anomalous momentum-dependence exists on the contact point at $\mathbf{k} = \pm\mathbf{k}_0$, while the total charge density $n(\mathbf{k}) = \sum_\alpha n_\alpha(\mathbf{k})$ is independent of $\mathbf{k}$ at $T = 0$.

Figure 9 shows the momentum-dependences of $n_3(\mathbf{k})$ and $n_4(\mathbf{k})$. The anti-symmetric component is found in the vicinity of the center of symmetry $\mathbf{k} = \pm\mathbf{k}_0$ accompanied by the discontinuous jumps at $\mathbf{k} = \pm\mathbf{k}_0$. The tendency of the momentum-dependence in $n_3(\mathbf{k})$ is opposite to those of $n_1(\mathbf{k})$, $n_2(\mathbf{k})$, and $n_4(\mathbf{k})$. This fact indicates a relevance that the charge disproportionation of n_3 which is much smaller than 3/4 (hole-rich). The anomaly exists not only in the ZGS but also in the metallic state discussed in the previous section. The origin of this anomaly is related to the point-contact of two bands, and is the same as that of the velocity matrix $\mathbf{u}_{\gamma\gamma'}(\mathbf{k})$, i.e., due to the anomaly of the eigenvector $d_{\alpha\gamma}(\mathbf{k})$ discussed in §6.

6. Discussion and Summary

We discuss the relation between the new massless fermions and the charge disproportionation. The anomaly of the velocity matrix $\mathbf{u}_{\gamma\gamma'}(\mathbf{k})$ and that of the charge density $n_\alpha(\mathbf{k})$ originates from the property of the wave function. We examine the Hamiltonian

$$H^{(2)} = \begin{bmatrix} a & c \\ c^* & b \end{bmatrix}, \quad (21)$$

which consists of two sites in a unit cell. ($a = b = 0$ and $c = k_x - ik_y$ in the case of graphite.[7]) When $\mathbf{k} = \mathbf{k}_0$, the diagonal components become equal ($a = b$) and the off-diagonal components vanish ($c = 0$) at the contact point of two bands. The components of the wave function depend on the phase θ, where $c = |c|e^{i\theta}$, i.e., θ is the angle of rotation around $\mathbf{k}_0$. The anomaly is discussed in terms of the helisity of neutrino in graphite, i.e., the pseudo spin vector describing the wave function is always parallel to the momentum $\mathbf{k}$.[9] The phase of the wave function jumps from θ to $\theta + \pi$ when $\tilde{\mathbf{k}}$ passes the contact point $\mathbf{k}_0$ into $-\tilde{\mathbf{k}}$. Such anomaly is an intrinsic property of the massless fermions.

Here the instability of the massless fermions in the presence of the site potential is also understood by using $H^{(2)}$. The diagonal components, which have different values in the presence of the site potential, violate the condition for degeneration. Thus the massless fermions in the presence of the charge disproportionation can not exist in the system which consists of two sites in a unit cell. In the case for α-(BEDT-TTF)$_2$I$_3$, the stability of the massless fermions is robust in the presence of the site potential. It is due to the electronic system with four sites in a unit cell, since diagonal components in 4×4 matrix with slightly different values allow degeneracy of eigenvalues. The velocity matrix $\mathbf{u}_{\gamma\gamma'}(\mathbf{k})$ and the charge density $n_\alpha(\mathbf{k})$ have the anomaly in both the amplitude and the phase, which are related to the charge disproportionation. Thus the correlation between the massless fermions and the charge disproportionation gives rise to a unique property of α-type salts which consists of four sites in a unit cell.

In summary, we have found that the Hamiltonian describing the massless fermions in α-(BEDT-TTF)$_2$I$_3$ has intrinsically new terms for σ_z and the identity matrix σ_0 in addition to the Weyl equation with σ_x and σ_y. The massless fermions in the present case have the anisotropy of the velocity and the inclination of the cone. Within the extrapolation scheme of the transfer integrals, we have found the pair of the contact points $\pm\mathbf{k}_0$ are merged to disappear at a high pressure, which is accompanied by strong anisotropy of the velocity and by the Van Hove singularities. The new massless fermions have robust stability against the charge disproportionation. The charge disproportionation originates from the variety of transfer integrals, while the spatial variation observed by the NMR experiment[25] is explained by taking account into the interactions. The anomalous momentum-dependence of the charge density in the vicinity of $\pm\mathbf{k}_0$ have been also found. The anomaly is due to the property of the wave function of the massless fermions, and is related to the charge disproportionation through the unitary matrix for the diagonalization.

Recently, anomalous three-stepwise structure in the magnetoresistance and enhancement of $1/T_1T$ in the NMR have been observed in the ZGS under magnetic field and high pressure in α-(BEDT-TTF)$_2$I$_3$,[17,29] while the two-stepwise structure has been observed in bismuth and graphite.[30] It is expected that these phenomena are related to the electronic states of the new massless Fermion. The roles of the new terms for σ_z and σ_0 on the magnetic response are interesting problems. It is also expected that the incorporation of the pair of the contact points $\pm\mathbf{k}_0$ at high pressure induces new phenomena.

Acknowledgments

This work has been financially supported by a Grant-in-Aid for Special Coordination Funds for Promoting Science and Technology (SCF) from the Ministry of Education, Culture, Sports, Science and Technology in Japan, and for Scientific Research on Priority Areas of Molecular Conductors (No. 15073213) from the Ministry of Education, Culture, Sports, Science and Technology in Japan.

1) J. M. Luttinger and W. Kohn: Phys. Rev. **97** (1955) 869.
2) P. A. Wolff: J. Phys. Chem. Solids **25** (1964) 1057.
3) H. Fukuyama and R. Kubo: J. Phys. Soc. Jpn. **28** (1970) 570.
4) H. Kohno, H. Yoshioka, and H. Fukuyama: J. Phys. Soc. Jpn. **61** (1992) 3462.
5) J. W. McClure: Phys. Rev. **104** (1956) 666.
6) J. C. Slonczewski and P. R. Weiss: Phys. Rev. **109** (1958) 272.
7) H. Ajiki and T. Ando: J. Phys. Soc. Jpn. **62** (1993) 1255.
8) T. Ando, T. Nakanishi, and R. Saito: J. Phys. Soc. Jpn. **67** (1998) 2857.
9) T. Ando: J. Phys. Soc. Jpn. **74** (2005) 777.
10) K. S. Novoselov, A. K. Geim, S. V. Morozov, D. Jiang, M. I. Katsnelson, I. V. Grigorieva, S. V. Dubonos, and A. A. Firsov: Nature **438** (2005) 197.
11) A. Kobayashi, S. Katayama, K. Noguchi, and Y. Suzumura: J. Phys. Soc. Jpn. **73** (2004) 3135.
12) S. Katayama, A. Kobayashi, and Y. Suzumura: J. Phys. Soc. Jpn. **75** (2006) 054705.
13) R. Kondo, S. Kagoshima, and J. Harada: Rev. Sci. Instrum. **76** (2005) 093902.
14) S. Ishibashi, T. Tamura, M. Kohyama, and K. Terakura: J. Phys. Soc. Jpn. **75** (2006) 015005.
15) H. Kino and T. Miyazaki: J. Phys. Soc. Jpn. **75** (2006) 034704.
16) K. Kajita, T. Ojiro, H. Fujii, Y. Nishio, H. Kobayashi, A. Kobayashi, and R. Kato: J. Phys. Soc. Jpn. **61** (1992) 23.
17) N. Tajima, S. Sugawara, M. Tamura, Y. Nishio, and K. Kajita: J. Phys. Soc. Jpn. **75** (2006) 051010.
18) S. Katayama, A. Kobayashi, and Y. Suzumura: J. Phys. Soc. Jpn. **75** (2006) 023708.
19) T. Takahashi: Synth. Met. **133–134** (2003) 261.
20) H. Kino and H. Fukuyama: J. Phys. Soc. Jpn. **64** (1995) 4523.
21) H. Seo: J. Phys. Soc. Jpn. **69** (2000) 805.
22) C. Hotta: J. Phys. Soc. Jpn. **72** (2003) 840.
23) N. Tajima, A. Ebina-Tajima, M. Tamura, Y. Nishio, and K. Kajita: J. Phys. Soc. Jpn. **71** (2002) 1832.
24) A. Kobayashi, S. Katayama, and Y. Suzumura: J. Phys. Soc. Jpn. **74** (2005) 2897.
25) S. Moroto, K.-I. Hiraki, Y. Takano, Y. Kubo, T. Takahashi, H. M. Yamamoto, and T. Nakamura: J. Phys. IV **114** (2004) 339.
26) H. Seo, C. Hotta, and H. Fukuyama: Chem. Rev. **104** (2004) 5005.
27) T. Mori, A. Kobayashi, Y. Sasaki, H. Kobayashi, G. Saito, and H. Inokuchi: Chem. Lett. (1984) 957.
28) H. Fukuyama: unpublished.
29) A. Shiomi, S. Yoshizaki, T. Nakamura, T. Takahashi, and K. Murata: Synth. Met. **86** (1997) 1975.
30) Y. Kopelevich, J. C. Medina Pantoja, R. R. da Silva, and S. Moehlecke: Ann. Phys. (N.Y.) **321** (2006) 1575.